Appl. Phys. A (2015) 121:51–57
DOI 10.1007/s00339-015-9311-0

Applied Physics A
Materials Science & Processing

Solution-combustion synthesized aluminium-doped spinel ($LiAl_xMn_{2-x}O_4$) as a high-performance lithium-ion battery cathode material

Mesfin A. Kebede[1] · Maje J. Phasha[2] · Niki Kunjuzwa[1,3] · Mkhulu K. Mathe[1] · Kenneth I. Ozoemena[1,3]

Received: 11 March 2015 / Accepted: 22 June 2015 / Published online: 29 June 2015

Abstract High-performing $LiAl_xMn_{2-x}O_4$ ($x = 0$, 0.125, 0.25, 0.375, and 0.5) spinel cathode materials for lithium-ion battery were developed using a solution combustion method. The as-synthesized cathode materials have spinel cubic structure of $LiMn_2O_4$ without any impurity peak and accompanied with peak shift as doping with aluminium. $LiAl_{0.375}Mn_{1.625}O_4$ (first cycle capacity = 113.1 mAh g^{-1}) retains 85 % (96.2 mAh g^{-1}), while pristine $LiMn_2O_4$ electrode (first cycle capacity = 135.8 mAh g^{-1}) fades quickly and retains only 54 % (73.9 mAh g^{-1}) after 50 cycles. The electrochemical performance of all the cathode samples prepared using the SCM is comparable to those reported for Al-doped $LiMn_2O_4$ spinel cathode materials. The experimental lattice parameter of $LiAl_xMn_{2-x}O_4$ was validated by ab initio calculations and correlated with the first cycle capacity of materials. The variation in lattice parameter as a result of Al doping greatly enhanced the cyclability of discharge capacity of the $LiMn_2O_4$ spinel.

1 Introduction

$LiMn_2O_4$ spinel is a promising material for the positive (cathode) electrode in rechargeable lithium-ion batteries. It has attracted a lot of research interest because of its several advantages such as low cost, high abundance, low toxicity, simplicity of preparation, and high safety compared with other layered oxides such as $LiCoO_2$ and $LiNiO_2$ [1, 2]. However, the problem with spinel $LiMn_2O_4$ cathode material is its rapid capacity fading upon repeated charge/discharge cycling [3, 4]. Some of the causes for the capacity fade of spinel cathode materials when used as battery materials include two-phase unstable reaction [5], dissolution of spinel into the electrolyte, and decomposition of the electrolyte in the 4 V region [6] and Jahn–Teller distortion in the 3 V region [7]. One of the strategies to retain capacity is by substitution of small amount of Mn ions by dopant ions such as Al, Ni [3, 7–9], and microwave irradiation [14]. It is believed that the dopant ions occupy the octahedral 16d sites of Mn ions in the spinel lattice and stabilize the spinel structure from lattice distortion. Homogeneous dispersion of the Mn^{3+} substituting element in crystal lattice is crucial in the synthesis of doped $LiMn_2O_4$ cathode materials. Hence, generally, solution synthesis techniques are preferable in order to get the required homogeneously doped composition. Up to now, several solution synthesis methods have been used to synthesize pristine $LiMn_2O_4$ spinel structure cathode material for rechargeable lithium-ion batteries, such as sol–gel method [10], emulsion-drying method [11], and combustion method [12, 13]. However, there are few reports where Al-doped $LiMn_2O_4$ is obtained using the solution combustion method [14]. The solution combustion method (SCM) allows for rapid synthesis of highly substituted oxides in a one-step process. SCM simply involves the use of aqueous solution of metal precursors (typically nitrates serving as oxidizers) mixed with fuel (e.g. hydrazine, glycine, or urea) and heated to self-ignition to yield complex oxides. When compared to other solution methods, SCM possesses a unique advantage of the quasi-atomic

✉ Mesfin A. Kebede
mkebede@csir.co.za

[1] Energy Materials, Materials Science and Manufacturing, Council for Scientific and Industrial Research (CSIR), Pretoria 0001, South Africa

[2] Transnet Rail Engineering, 160 Lynette Street, Pretoria, South Africa

[3] School of Chemistry, University of the Witwatersrand, Private Bag 3, P O WITS 2050, Johannesburg, South Africa

dispersion of the component cations in liquid precursors, which facilitates synthesis of the crystallized powder with low particle size and high purity at low temperatures [15].

In this paper, we have synthesized $LiMn_2O_4$ spinel and its aluminium-doped counterparts ($LiAl_xMn_{2-x}O_4$, where $x = 0.125$, 0.25, 0.375, and 0.5) following the SCM using metal nitrates and urea as a fuel through an exothermic and self-sustaining chemical reaction. In addition, we report the correlation between the first cycle discharge capacity and lattice parameter of Al-doped spinel $LiMn_2O_4$ using experimental data analyses validated by ab initio first-principles calculations. The lithium intercalation energy of the pristine and aluminium-doped $LiMn_2O_4$ cathode materials are calculated using CASTEP code incorporated within Materials Studio software [16, 17].

2 Experimental

2.1 Materials and synthesis of $LiAl_xMn_{2-x}O_4$ spinel cathode materials

Similar to a previous study [18], the synthesis of $LiAl_xMn_{2-x}O_4$ spinel cathode materials for Li-ion battery was carried out in a furnace using 99.9 % pure $Li(NO_3)$, $Mn(NO_3)_2{\cdot}4H_2O$, $Al(NO_3)_3{\cdot}9H_2O$, and urea ($(NH_2)_2CO$) as starting materials. All the precursors were obtained from Sigma-Aldrich. The stoichiometric compositions of the redox mixtures for the combustion reaction are calculated using the total oxidizing and reducing valencies of the components to obtain the maximum energy released during the combustion process.

Accordingly, based on the stoichiometric ratios, appropriate masses of the precursor materials (see Table 1) were dissolved into 20 mL of deionized water in a 100-mL beaker and stirred at ambient temperature for about 30 min to obtain homogeneously mixed solution. After that, the precursor solution was introduced into a furnace, preheated at 500 °C, and the exothermic reaction took place and completed within 10 min to obtain a black powdered product. And then finally the product powder was calcined at 700 °C for 10 h to form spinel $LiMn_2O_4$ crystal structure. To investigate the effect of Al ion on the structural and electrochemical properties of $LiMn_2O_4$ cathode materials, Al-doped samples (with Al-ion concentration of 0.125, 0.25, 0.375, and 0.5) were prepared under atmospheric pressure and then calcined at 700 °C in air for 10 h. The voluminous and foamy combustion ash was easily milled to obtain the final $LiAl_xMn_{2-x}O_4$ cathode materials. The tap density of the as-synthesized $LiMn_2O_4$ materials, determined using the graduated measuring cylinder method, was about 1.41 g cm^{-3}.

2.2 Equipment and procedure

The structural properties of the samples were investigated by X-ray diffraction analysis using a PANalytical X'Pert PRO PW3040/60 X-ray diffractometer with Fe-filtered Cu-Kα ($\lambda = 1.5479026$ nm) monochromated radiation source. Data were collected in the 2θ range of 10°–90° at a scan rate of 2 °/min. The morphology of the products was obtained using a high-resolution scanning electron microscope (JEOL, JSM-7600F, operated at an accelerating voltage of 5 kV). The lattice parameters of the synthesized spinels, obtained from the XRD, were further corroborated from ab initio calculations using CASTEP code [16, 17], which is a *first-principles* quantum mechanical programme based on the Hohenberg–Kohn–Sham density functional theory (DFT) [19–21], used within the generalized gradient approximation (GGA) formalism [22] to describe the electronic exchange–correlation interactions. We employed the spin-polarized PW91 [23] functional of GGA. Within CASTEP, maximum plane wave cut-off energy of 500 eV using Vanderbilt-type ultrasoft (US) pseudopotentials [24] and $3 \times 3 \times 3$ Monkhorst–Pack [25] k-point mesh were applied on a conventional unit cell with P1 symmetry. Geometry optimization was conducted using the Broyden–Fletcher–Goldfarb–Shanno (BFGS) method [26]. We have used this approach in our previous report for small Al content [27], while in this study we consider large Al content.

2.3 Electrochemical characterization

Coin cells of 2032 configuration were assembled using lithium metal as anode, Celgard 2400 as separator, 1 M

Table 1 Mass of the precursor materials in gram calculated according to the stoichiometric ratio

Sample	Mass of precursor materials used in the synthesis (g)			
	$LiNO_3$	$Mn(NO_3)_2{\cdot}4H_2O$	$Al(NO_3)_3{\cdot}9H_2O$	$(NH_2)_2CO$
$LiMn_2O_4$	0.550	4.000	0	1.435
$LiAl_{0.125}Mn_{1.875}O_4$	0.550	3.750	0.370	1.435
$LiAl_{0.25}Mn_{1.75}O_4$	0.550	3.500	0.750	1.435
$LiAl_{0.375}Mn_{1.625}O_4$	0.550	3.250	1.120	1.435
$LiAl_{0.5}Mn_{1.5}O_4$	0.550	3.000	1.500	1.435

solution of $LiPF_6$ in 50:50 (v/v) mixture of ethylene carbonate (EC) and diethylene carbonate (DEC) as the electrolyte. The cathode was made through a slurry coating procedure from a mixture containing active material powder, conducting black and poly(vinylidene fluoride) binder in *N*-methyl-2-pyrrolidone in the proportion 80:10:10, respectively. The slurry was coated over aluminium foil and dried at 120 °C for 10 h in vacuum oven under vacuum condition. Then, 18-mm-diameter slurry-coated aluminium foils electrodes were punched out and used as cathode. Coin cells were assembled in an argon-filled glove box (MBraun, Germany) with moisture and oxygen levels maintained at <1 ppm. The cells were cycled at 0.2 C rate at room temperature with respect to corresponding theoretical capacities of $LiAl_xMn_{2-x}O_4$ spinel between 2.4 and 4.8 V in an MTI a multichannel battery tester.

3 Results and discussion

3.1 Morphology and structural characterization

Figure 1a–d show typical SEM images of $LiAl_xMn_{2-x}O_4$ for $x = 0$, 0.125, 0.25, and 0.375 samples, respectively. It is clearly seen that the morphology of the as-synthesized powders is satisfactorily dispersed, reflecting the inherent nature of the combustion process (insets of Fig. 2b–d). The surfaces of the foams show a lot of voids and pores caused by the escaping gases during combustion reaction. The particles have regular shapes with well-defined faces, and the microstructure obtained indicates the high crystallinity of the as-synthesized product powder. Using the SEM images, the estimated particle size range for the compositions $x = 0$, $x = 0.125$, $x = 0.25$, $x = 0.375$, and $x = 0.5$, respectively, is 475 nm–2.2 μm, 200–525 nm, 200–800 nm, 300–800 nm, and 200–700 nm. The aluminium-doped samples are small in size compared with pristine $LiMn_2O_4$, in agreement with the literature report [14].

Figure 2a compares typical XRD pattern of each sample as a function of aluminium concentration. The examination of the diffraction patterns confirms that all recognizable reflection peaks including (111), (311), (222), (400), (331), (511), (440), (531), (533), (622), (551), and (731) can be clearly indexed to the single phase of the spinel cubic structure of $LiMn_2O_4$ (JCPDS File No. 88-1749) with space group Fd-3m, without any impurity peaks. The doped Al^{3+} mostly occupies octahedral Mn site (16d) and enhances the cyclability by stabilizing the spinel structure. However, there is optimal amount of Al-ion doping that increases the structural stability of $LiMn_2O_4$. This Al doping of spinel $LiMn_2O_4$ increases the mean Mn valence, but exceeding the critical concentration of Al might hinder

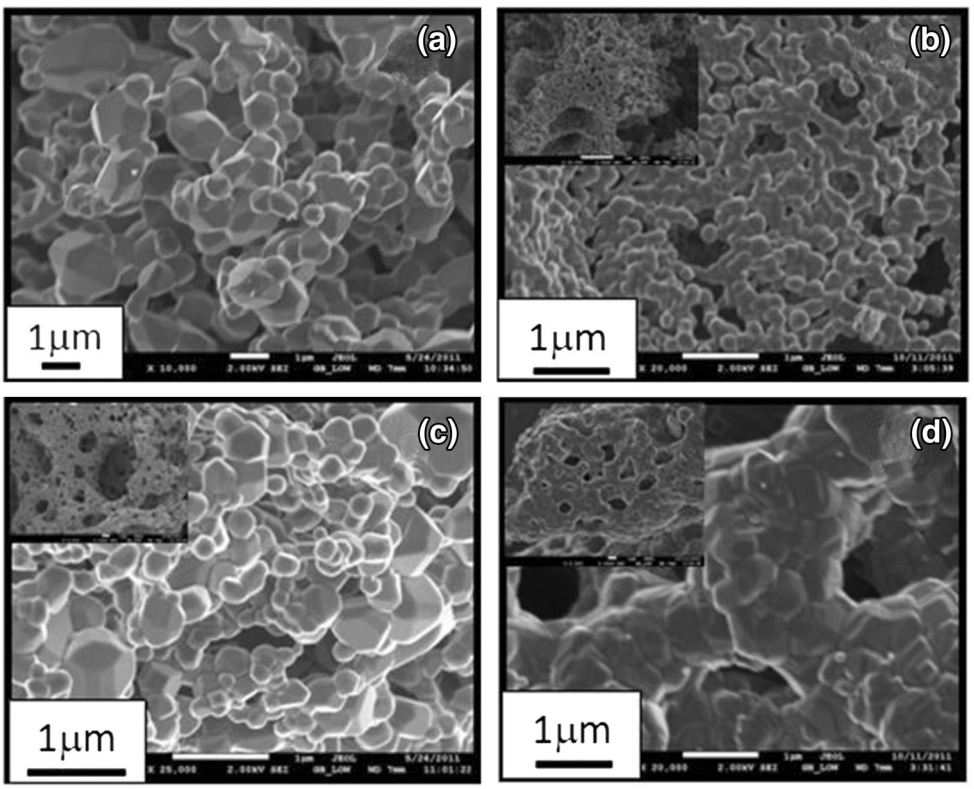

Fig. 1 SEM images of $LiAl_xMn_{2-x}O_4$ cathode materials for **a** $x = 0$, **b** $x = 0.125$, **c** $x = 0.25$, and **d** $x = 0.375$

the Li movement by occupying the Li site resulting in unacceptable low capacity. In our samples the optimized aluminium concentration to get a reasonable capacity and cyclability is $x = 0.375$. Figure 2b shows the peak shift of (111) plane towards higher angle for the samples $LiMn_2O_4$, $LiAl_{0.25}Mn_{1.75}O_4$, and $LiAl_{0.5}Mn_{1.5}O_4$ as the lattice structure of $LiMn_2O_4$ shrinks due to efficient Al doping.

Table 2 compares the lattice parameters (a-value/Å and unit cell volume/Å^3) of the pristine and Al-doped spinel materials. The calculated values from the XRD follows same trend with the ab initio calculation. As the amount of aluminium is increased, the lattice parameter is decreased.

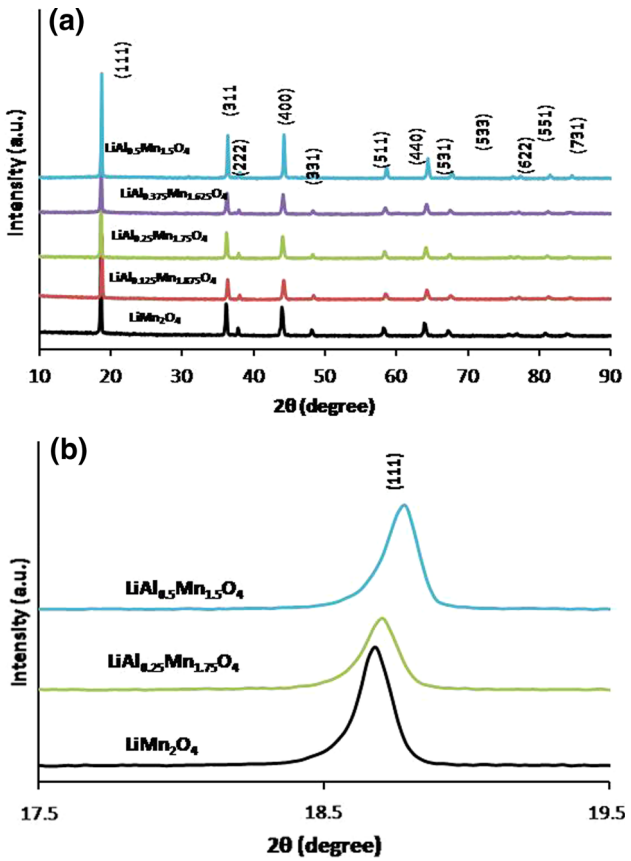

Fig. 2 **a** X-ray diffraction pattern of $LiAl_xMn_{2-x}O_4$ cathode materials (where $x = 0$, 0.125, 0.25, 0.375, and 0.5) **b** (111) plane peak shift for $x = 0$, 0.25, and 0.5

This is expected considering that there is increase in the concentration of small Mn^{4+} (0.53 Å) ions in the spinel structure as big Mn^{3+} (0.645 Å) ions are substitutes by smaller Al^{3+} (0.53 Å) ions.

3.2 Electrochemical characterization

Generally, the theoretical capacity, C_T, can be expressed as follows [28]:

$$C_T = 26.8p/M \quad (1)$$

where p and M denote the number of Mn(III) and the molecular weight of ion-doped $LiMn_2O_4$, respectively. Employing Eq. (1), the theoretical capacity of $LiAl_xMn_{2-x}O_4$ is found to be 148, 132.2, 115.6, 98.3, and 80.3 mAh g^{-1} for $x = 0$, $x = 0.125$, $x = 0.25$, $x = 0.375$, and $x = 0.5$, respectively. We have carried out the galvanostatic charge–discharge capacity performance testing of the cathode materials at 0.2 C rates with respect to their corresponding theoretical capacities. The representative first cycle discharge capacities of $LiAl_xMn_{2-x}O_4$ ($x = 0$, 0.125, 0.25, 0.375, and 0.5) are presented in Fig. 3A, B, C, D, and E, respectively. During the first cycle pristine $LiMn_2O_4$ delivers discharge capacity of 135.8 mAh g^{-1}, $LiAl_{0.125}Mn_{1.875}O_4$ gives 134.8 mAh g^{-1}, $LiAl_{0.25}Mn_{1.75}O_4$ about 111.5 mAh g^{-1}, $LiAl_{0.375}Mn_{1.625}O_4$ around 113.1 mAh g^{-1}, and $LiAl_{0.5}Mn_{1.5}O_4$ about 95.2 mAh g^{-1} which are comparable to their theoretical values. Our results are exhibiting superior capacity when compared to aluminium-doped $LiMn_2O_4$ cathode materials synthesized using sol–gel methods [29, 30]. Our $LiMn_2O_4$ cathode material using combustion method has relatively performed better (initial capacity of 135.8 mAh g^{-1} and retains 54 % after 50 cycle), as we observe the recent report by Zhang et al. [31] which gave them initial capacity of 118.6 mAh g^{-1} and 33.2 % capacity retention after 50 cycles. All the cathode samples prepared using the SCM are well-performing materials. Hence, synthesizing spinel using urea as fuel via SCM yields high-performing material.

The trend of the first cycle discharge capacity of the $LiAl_xMn_{2-x}O_4$ cathode materials in relation to the aluminium content is displayed in Fig. 4a. The first cycle

Table 2 Structural parameters obtained for the $LiAl_xMn_{2-x}O_4$ ($x = 0$, 0.125, 0.25, 0.375, and 0.5) samples from both XRD (Rietveld refinement) and DFT calculations

Sample	XRD Rietveld refinement		DFT calculation	
	a (Å)	Unit cell volume (Å^3)	a (Å)	Unit cell volume (Å^3)
$LiMn_2O_4$	8.2242	556.264	8.3232	576.595
$LiAl_{0.125}Mn_{1.875}O_4$	8.2231	556.041	8.3228	576.512
$LiAl_{0.25}Mn_{1.75}O_4$	8.2099	553.367	8.28	567.664
$LiAl_{0.375}Mn_{1.625}O_4$	8.2086	553.105	8.26	563.559
$LiAl_{0.5}Mn_{1.5}O_4$	8.1757	546.480	8.24	559.476

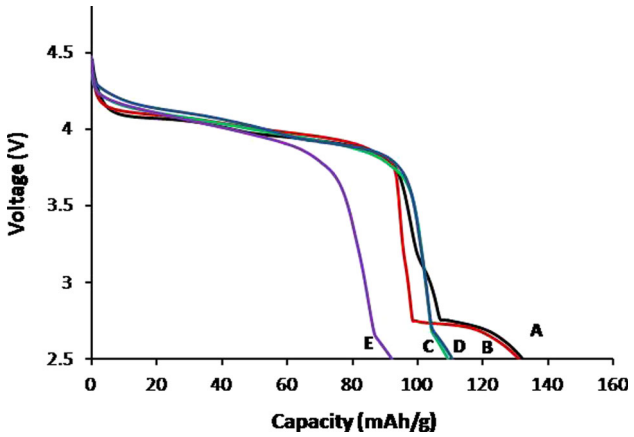

Fig. 3 First cycle discharge capacity curves of $LiAl_xMn_{2-x}O_4$ cathode materials *A*, *B*, *C*, *D*, and *E* for $x = 0$, 0.125, 0.25, 0.375, and 0.5, respectively, at the C-rate = 0.2 C

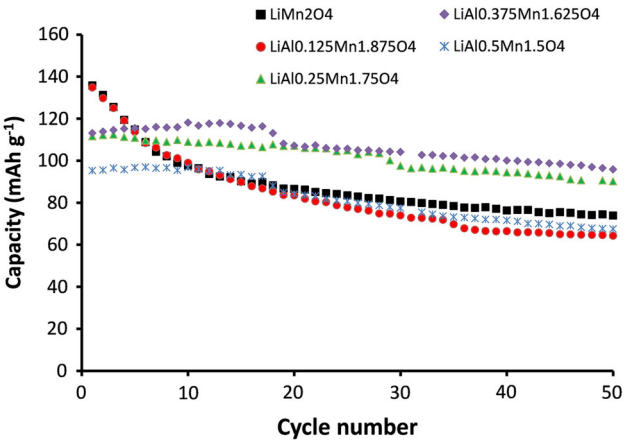

Fig. 5 Discharge capacity cycling performance of $LiAl_xMn_{2-x}O_4$ samples for the first 50 cycles at the C-rate = 0.2 C

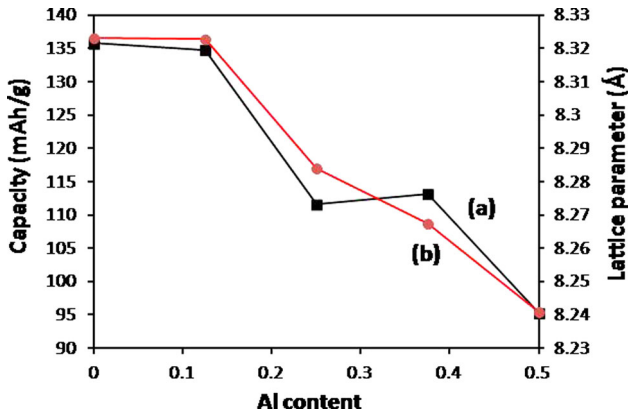

Fig. 4 **a** First cycle discharge capacity of $LiAl_xMn_{2-x}O_4$, and **b** the calculated lattice parameter of the composition $LiAl_xMn_{2-x}O_4$ ($x = 0$, 0.125, 0.25, 0.375, and 0.5)

discharge capacity of pristine $LiMn_2O_4$ and $LiAl_{0.125}Mn_{1.875}O_4$ samples did not vary significantly. Also, as displayed in Fig. 4b, the calculated lattice parameter of $LiAl_{0.125}Mn_{1.875}O_4$ (8.3228 Å) is almost equal to the lattice parameter of pristine $LiMn_2O_4$ (8.3232 Å). These experimental and theoretical results indicate that both pristine $LiMn_2O_4$ and small Al-content-doped $LiAl_{0.125}Mn_{1.875}O_4$ samples exhibit high first cycle discharge capacity and larger lattice parameters compared with other high Al-content-doped samples. The larger the lattice parameter, the easier the Li ions can move more freely [32–34], thereby increasing the discharge capacity. As expected, beyond $x = 0.125$ (in our case for $x = 0.25$, 0.375, and 0.5) the first cycle discharge capacity of the doped $LiMn_2O_4$ cathode material becomes much less than that of the pristine $LiMn_2O_4$. The calculated lattice parameter for the samples with $x = 0.25$, $x = 0.375$, and $x = 0.5$ decreased to 8.28, 8.26, and 8.24 Å, respectively. A higher degree of Al doping can therefore be correlated with a decreased lattice parameter, which in turn leads to a lower discharge capacity. This finding indicates that the discharge capacity is not only correlated exclusively to the molecular weight of ion-doped $LiMn_2O_4$, but also to its lattice parameter.

Figure 5 compares the cyclability of the $LiAl_xMn_{2-x}O_4$ samples upon 50 repetitive cycles. The discharge capacity of $LiMn_2O_4$ and $LiAl_{0.125}Mn_{1.875}O_4$ fades faster compared with the other samples. This figure depicts the effect of Al-ion content on the cycling performance of $LiMn_2O_4$. It can be seen that the curve of $LiAl_{0.375}Mn_{1.625}O_4$ has a maximum cycling stability, which is about 1.6 times that of the cycling stability of undoped $LiMn_2O_4$ after 50 cycles. Our result agrees with Julien et al. [35] who reported that $LiAl_{0.3}Mn_{1.7}O_4$ has a better cyclability than $LiAl_{0.1}Mn_{1.9}O_4$. We surmise that the composition $LiAl_{0.375}Mn_{1.625}O_4$ suppressed the effect of Jahn–Teller distortion and that the concentration of Mn^{3+} which induces Jahn–Teller distortion in the spinel is decreased.

Figure 6a represents the change in discharge capacity (50th cycle discharge capacity/first discharge capacity) for the $LiAl_xMn_{2-x}O_4$ cathode materials. Compared with the pristine $LiMn_2O_4$ cathode material, the $LiAl_{0.125}Mn_{1.875}O_4$ composition did not improve the cyclability, whereas the other doped spinel compositions do retain their initial capacities for many cycles; for example, aluminium-doped compositions $LiAl_{0.25}Mn_{1.75}O_4$, $LiAl_{0.375}Mn_{1.625}O_4$, and $LiAl_{0.5}Mn_{1.5}O_4$, respectively, retain 1.5, 1.6, and 1.3 times that of pristine $LiMn_2O_4$. It is apparent that the samples with Al-ion concentration of $x = 0.375$ exhibit higher capacity retention about 85 % after 50 cycles. The enhanced cyclability of the sample $LiAl_{0.375}Mn_{1.625}O_4$ in the present study is primarily attributed to the optimum Al-ion doping which results in stabilizing the spinel structure.

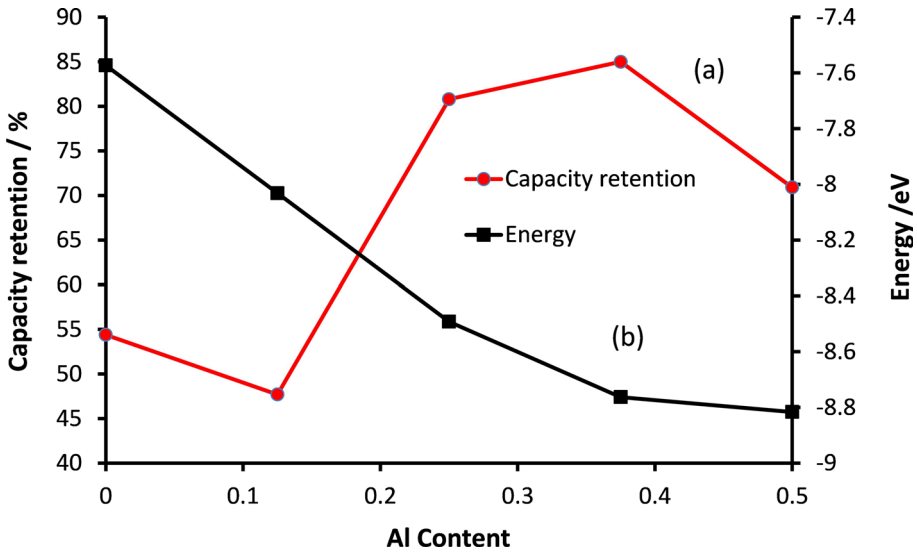

Fig. 6 **a** Discharge capacity retention of $LiAl_xMn_{2-x}O_4$ after 50 cycles at C-rate = 0.2 C, **b** the computational intercalation energy per Li atom

The observed stability trends are further validated by ab initio predictions in Fig. 6b, c. As shown in Fig. 6b, an increase in Al-dopant corresponds to more negative intercalation energy which implies easy Li-ion movement. On the other hand, this increase in Al yields higher average open-circuit voltage of up to approximately 4.8 when $x = 0.5$.

4 Conclusion

We have synthesized $LiAl_xMn_{2-x}O_4$ cathode materials for Li-ion battery using metal nitrates and urea as precursors by solution combustion method. The samples were characterized by SEM, XRD, and charge/discharge battery tester. The first cycle discharge capacity of $LiAl_{0.125}Mn_{1.875}O_4$ is comparable to that of the pristine $LiMn_2O_4$, just as the values of their lattice parameter are essentially the same. In addition, the $LiAl_{0.375}Mn_{1.625}O_4$ sample exhibited the more stable discharge capacity than the other samples. The variation in lattice parameter as a result of Al doping greatly enhanced the cyclability of discharge capacity of the $LiMn_2O_4$ spinel.

Acknowledgments We thank the CSIR for supporting this work. MK would like to acknowledge the NRF for supporting this work financially.

References

1. A.S. Arico, P. Bruce, B. Scrosati, J.M. Tarascon, W. Van Schalkwijk, Nat. Mater. **4**, 366 (2005)
2. H. Şahan, H. Göktepe, Ş. Patat, A. Ülgen, J. Alloys Compd. **509**, 4235 (2011)
3. A. Yuan, L. Tian, W. Xu, Y. Wang, J. Power Sources **195**, 5032 (2010)
4. M. Prabu, M. Reddy, S. Selvasekarapandian, G.S. Rao, B. Chowdari, Electrochim. Acta **88**, 745 (2013)
5. W. Zhou, S. Bao, B. He, Y. Liang, H. Li, Electrochim. Acta **51**, 4701 (2006)
6. L. Xiao, Y. Zhao, Y. Yang, Y. Cao, X. Ai, H. Yang, Electrochim. Acta **54**, 545 (2008)
7. T. Yi, Y. Zhu, R. Zhu, L. Zhou, P. Li, J. Shu, Ionics **15**, 177 (2009)
8. R. Thirunakaran, A. Sivashanmugam, S. Gopukumar, R. Rajalakshmi, J. Power Sources **187**, 565 (2009)
9. D. Guo, B. Li, Z. Chang, H. Tang, X. Xu, K. Chang, E. Shangguan, X. Yuan, H. Wang, Electrochim. Acta **134**, 338 (2014)
10. C.J. Curtis, J. Wang, D.L. Schulz, J. Electrochem. Soc. **151**, A590 (2004)
11. S. Myung, S. Komaba, N. Kumagai, J. Electrochem. Soc. **148**, A482 (2001)
12. K. Lee, H. Choi, J. Lee, J. Mater. Sci. Lett. **20**, 1309 (2001)
13. C. Peng, H. Bai, Q. Li, Y. Guo, J. Huang, C. Su, J. Guo, Int. J. Electrochem. Sci. **10**, 3885 (2015)
14. F.P. Nkosi, C.J. Jafta, M. Kebede, L. le Roux, M.K. Mathe, K.I. Ozoemena, RSC Adv. **5**, 32256 (2015)
15. K.C. Stella, A.S. Nesaraj, Iran. J. Mater. Sci. Eng. **7**, 36 (2010)
16. M. Segall, P.J.D. Lindan, M. Probert, C. Pickard, P. Hasnip, S. Clark, M. Payne, J. Phys. Condens. Matter **14**, 2717 (2002)
17. S.J. Clark, M.D. Segall, C.J. Pickard, P.J. Hasnip, M.I.J. Probert, K. Refson, M.C. Payne, Z. Kristallogr. **220**, 567 (2005)
18. M.A. Kebede, N. Kunjuzwa, C.J. Jafta, M.K. Mathe, K.I. Ozoemena, Electrochim. Acta **128**, 172 (2014)
19. P. Hohenberg, W. Kohn, Phys. Rev. **136**, B864 (1964)
20. W. Kohn, L.J. Sham, Phys. Rev. **140**, A1133–A1138 (1965)
21. P. Hohenberg, W. Kohn, Phys. Rev. **136**, B864 (1964)
22. J.P. Perdew, Y. Wang, Phys. Rev. B **45**, 13244 (1992)
23. J.P. Perdew, J. Chevary, S. Vosko, K.A. Jackson, M.R. Pederson, D. Singh, C. Fiolhais, Phys. Rev. B **46**, 6671 (1992)
24. D. Vanderbilt, Phys. Rev. B **41**, 7892 (1990)
25. H.J. Monkhorst, J.D. Pack, Phys. Rev. B **13**, 5188 (1976)
26. T.H. Fischer, J. Almlof, J. Phys. Chem. **96**, 9768 (1992)
27. M.A. Kebede, M.J. Phasha, N. Kunjuzwa, L.J. le Roux, D. Mkhonto, K.I. Ozoemena, M.K. Mathe, Sustain. Energy Technol. Assess. **5**, 44 (2014)
28. T. Kakuda, K. Uematsu, K. Toda, M. Sato, J. Power Sources **167**, 499 (2007)

29. S.J. Bao, Y.Y. Liang, W.J. Zhou, B.L. He, H.L. Li, J. Power Sources **154**, 239 (2006)
30. R. Thirunakaran, A. Sivashanmugam, S. Gopukumar, C.W. Dunnill, D.H. Gregory, J. Mater. Process. Technol. **208**, 520 (2008)
31. H. Zhang, Y. Xu, D. Liu, X. Zhang, C. Zhao, Electrochim. Acta **125**, 225 (2014)
32. Y. Huang, R. Jiang, S.J. Bao, Y. Cao, D. Jia, Nanoscale Res. Lett. **4**, 353 (2009)
33. G. Amatucci, J.M. Tarascon, J. Electrochem. Soc. **149**, K31 (2002)
34. T. Tsumura, A. Shimizu, M. Inagaki, Solid State Ion. **90**, 197 (1996)
35. C. Julien, S. Ziolkiewicz, M. Lemal, M. Massot, J. Mater. Chem. **11**, 1837 (2001)